We are IntechOpen,
the world's leading publisher of
Open Access books
Built by scientists, for scientists

6,700
Open access books available

180,000
International authors and editors

195M
Downloads

Our authors are among the

154
Countries delivered to

TOP 1%
most cited scientists

12.2%
Contributors from top 500 universities

CLARIVATE ANALYTICS
BOOK CITATION INDEX
INDEXED

WEB OF SCIENCE™

Selection of our books indexed in the Book Citation Index
in Web of Science™ Core Collection (BKCI)

Interested in publishing with us?
Contact book.department@intechopen.com

Chapter

Optimal Analysis for the Enhancement in the Thermal Variables Measurement by Smart and Modular Solid State Sensors

J. Alan Calderón Ch, Fernando O. Jiménez U.,
E. Benjamín Barriga G., Julio C. Tafur S., Dante J. Gallo T.,
Juan Carlos R. Lengua A., John H. lozano J. and
Hugo Lozano Núñez

Abstract

The proposed research aims to analyze and optimize the measurement of thermal physical variables during the operation of a hydrogen combustion engine. The optimal measurement of the flow, temperature, pressure, and volume is given over the hydrogen, which is the main fuel of the studied combustion motor. Hence, the success of the measurement is based on the polynomial analysis of the combustion motor operation, which needs nonlinear algorithms to get the optimal correlation of the measured physical variables as well as a high robustness and short response time during the transduction of the measured physical variable, which is achieved as a consequence of the anodic aluminum oxide (AAO) amorphous nanostructures properties that are modular solid state integration of the designed smart sensor. The short response time and high robustness is a good advantage for the designed smart sensor since it gives more time to execute sophisticated algorithms in order to get the optimal physical variables measurement. In fact, the proposed smart sensor keeps the possibility to be modular and solid state for the interaction with the hydrogen fuel as well as recognizing the presence of other molecules mixed in the fluid, which can alarm the user who is able to recognize whether it is joined oxygen or carbon residues. Therefore, the proposed research work toward a good compromise to care for the environment condition based on a cleaner combustion motor operation.

Keywords: internal combustion motors (ICM), transducers, nanostructures, smart sensors, hydrogen

1. Introduction

There is a big responsibility regarding the combustion motors residual compromises, as well as caring their effects on pollution. Consequently, there were prepared

some agreements to get action over that problematic, for instance: "What could happen with the older busses and automobiles (which use ICM) in countries where it will not be easy to take them off them from the public/private transport?".

The described question above has not a simple answer, due to the fact that the public transport in many countries (such as in Latin-American) depends on very older ICM, even though there are expectations on new motors as part of the buses on public transport, which are based on electrical motors or hydrogen ICM. Nevertheless, changing their old transport will not be practical for many drivers, and it is expected that different adapted and hybrid systems will be prepared in order to provide adapted ICM with the capability to use hydrogen or different mixing of fuel. Otherwise, this will be trouble due to it must be warranted to get optimal systems to measure the good quality, purity, and concentration of the used fuel. For this reason, this research is proposed a smart sensor to measure the fuel flow with the possibility of giving information on the presence of oxygen or different hydrocarbon molecules.

Therefore, **Figure 1** represents the designed smart sensor as part of an ICM system, in which "φ1" means the input of fuel flow to the combustion motor "CM", from which it is possible to obtain torque "T" and revolution per minute "RPM" to be used for machines. Notwithstanding, inside the "CM" is fixed the designed smart sensor "SS" that receives the static difference of pressure "ΔP" that is achieved through the road of the flow on the transducers of "NS". In fact, the estimated signal obtained after the processing of the smart sensor can be sent to an external user through wireless (EW1).

Therefore, the designed smart sensor has the capability to identify fuel based on hydrogen, even though the sensitivity of their transducers also can identify the presence of either oxygen or some molecules of hydrocarbons, in order to give this information to the user through wireless or wire mechanisms [1–5]. That information is quite important to proportionate a diagnostic of the ICM operation, as well as the presence of molecules that can cause disturbance in the optimal operation, by other side the vibration of the motor can be also considered as some kind of disturbances quite important to be studied in the ICM analysis [6, 7].

2. Analysis of the fuel fluid mechanics for the designed smart sensor

In this chapter, the behavior of fluid is analyzed by classic interpretation, such as "the second Newton law," where a differential of mass is stored over a differential of
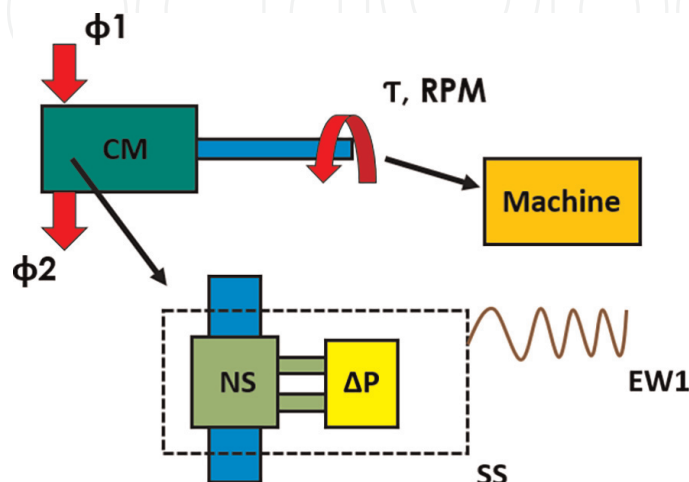

Figure 1.
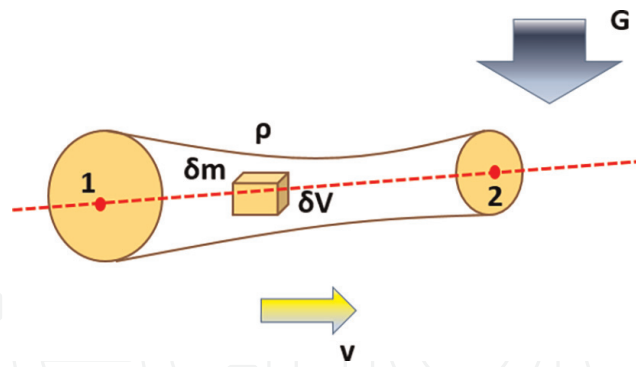*Smart sensor scheme.*

Figure 2.
Theoretical representation of a differential of mass and volume as part of a fluid.

volume by density "ρ", which is represented in **Figure 2**. This differential of mass is under gravity force (as a consequence of the gravity field "G"); moreover, the force is a consequence of the gradient of the pressure around the differential volume, since it must be interpreted in the fluid dynamic analysis from the point 1 to the point 2, as well as it is depicted in **Figure 2**.

The Eq. (1) gives the information over a mass differential "δm", which is supported by the Newton's second law due to get its dynamic analysis as a consequence of the speed "v", Cartesian space derivative over the pressure "P", differential volume "δV", volumetric forces "f and F", in which "f" is a consequence of an external cause that could be an electro valve, furthermore "F" is caused by gradient of "G" effects [8, 9]. Hence, the dynamic of the fluid described above is represented in the Eq. (1).

$$\delta m \frac{dv}{dt} + \left(\frac{\partial P}{\partial x}, \frac{\partial P}{\partial y}, \frac{\partial P}{\partial z} \right) \delta V = (f + F)\delta V \tag{1}$$

Eq. (1) was organized considering the fluid density "ρ" and the gradient of the pressure "P" to get Eq. (2) [8, 10, 11]:

$$\rho \delta V \frac{dv}{dt} + \nabla P \delta V = (f + F)\delta V \tag{2}$$

In order to get the gravity effect analysis over the differential of mass, F force is replaced with gradient G [8, 10, 11]:

$$F = \rho \left(\frac{\partial G}{\partial x}, \frac{\partial G}{\partial y}, \frac{\partial G}{\partial z} \right) \tag{3}$$

Hence, replacing Eq. (3) in Eq. (2), it was achieved Eq. (4) [8, 10, 11]:

$$\rho \delta V \frac{dv}{dt} + \nabla P \delta V = (f + \rho \nabla G)\delta V \tag{4}$$

In spite of, the previous Eq. (4), it was possible to obtain the external force "f," which can be useful for the simulation analysis according to get an understanding and applications of smart electro valves, as it is described by Eq. (5). Notwithstanding, this research is focused on smart sensor analysis [8, 10, 11]:

$$\rho \frac{dv}{dt} + \nabla P - \rho \nabla G = f \tag{5}$$

Therefore, in Eq. (2), for "f" equal to zero, it is obtained the Eq. (6) [8, 10, 11]:

$$\rho \delta V \frac{dv}{dt} = (F - \nabla P)\delta V \tag{6}$$

In addition, Eq. (6) is multiplied by the speed "v" in both of its members, owing to get an energy analysis model, which is given by Eq. (7) [8, 10, 11]:

$$\rho \delta V \frac{d\left(\frac{1}{2}v^2\right)}{dt} = v.(F - \nabla P)\delta V \tag{7}$$

Eqs. (8) and (9) are quite necessary to get reduction over Eq. (7), from which their demonstration is written in the appendix of this chapter [8, 10, 11]:

$$\frac{d}{dt} = \frac{\partial}{\partial t} + v.\nabla \tag{8}$$

$$\frac{d}{dt}\delta V = \delta V \nabla.v \tag{9}$$

From Eq. (8), it is analyzed its modeling over Eq. (7) reduction, which is given by Eq. (10) [8, 10, 11]:

$$\rho \delta V \frac{1}{2}\frac{dv^2}{dt} = v.F\delta V + \frac{\partial(P\delta V)}{\partial t} - \frac{d(P\delta V)}{dt} \tag{10}$$

It means that it is necessary to find a balance between the total derivative "$\frac{d}{dt}$" and the partial derivative "$\frac{\partial}{\partial t}$" on the time dependence, such as it is explained through Eq. (11) [8, 10, 11]:

$$\rho \delta V \frac{1}{2}\frac{dv^2}{dt} = v.F\delta V + \frac{\partial(P\delta V)}{\partial t} - \left[P\frac{d(\delta V)}{dt} + \delta V\frac{d(P)}{dt}\right] \tag{11}$$

Moreover, it was regrouped Eq. (11), owing to find the components on the dependence of time domain for total derivative as energy balance analysis, which is described by Eq. (12) [8, 10, 11]:

$$\rho \delta V \frac{1}{2}\frac{dv^2}{dt} + \delta V\frac{d(P)}{dt} - v.F\delta V = \frac{\partial(P\delta V)}{\partial t} - P\frac{d(\delta V)}{dt} \tag{12}$$

On the other hand, returning again the force F over the previous Eq. (12), Eq. (1) was achieved [8, 10, 11].

$$\rho \delta V \frac{1}{2}\frac{dv^2}{dt} + \delta V\frac{d(P)}{dt} - v.[-\rho\nabla G]\delta V = \frac{\partial(P\delta V)}{\partial t} - P\frac{d(\delta V)}{dt} \tag{13}$$

Additionally, using Eq. (8) on the previous Eq. (13), it is able to be obtained Eq. (14) [8, 10, 11]:

$$\rho \delta V \frac{1}{2} \frac{dv^2}{dt} + \delta V \frac{d(P)}{dt} + \rho [v.\nabla G] \delta V = \frac{\partial (P \delta V)}{\partial t} - P \frac{d(\delta V)}{dt} \qquad (14)$$

Hence, by Eq. (8) in Eq. (14), it was proposed, as a target, to find the total derivation as dependent on the time over the gravity effect for the mass differential on the fluid, which is given by Eq. (15) [8, 10, 11]:

$$\rho \delta V \frac{1}{2} \frac{dv^2}{dt} + \delta V \frac{d(P)}{dt} + \rho [v.\nabla G] \delta V = \frac{\partial (P \delta V)}{\partial t} - P \frac{d(\delta V)}{dt} \qquad (15)$$

Therefore, on Eq. (16) is possible to identify the total derivation as dependent on the time for the pressure and gravity effect over the mass differential of the analyzed fluid [8, 10, 11]:

$$\rho \delta V \frac{1}{2} \frac{dv^2}{dt} + \delta V \frac{d(P)}{dt} + \rho \left[\frac{dG}{dt} - \frac{\partial G}{\partial t} \right] \delta V = \frac{\partial (P \delta V)}{\partial t} - P \frac{d(\delta V)}{dt} \qquad (16)$$

It means that Eq. (17) separates in both members the total derivative on the time domain, in comparison to partial derivation on the time domain [8, 10, 11]:

$$\rho \delta V \frac{1}{2} \frac{dv^2}{dt} + \delta V \frac{d(P)}{dt} + \rho \frac{dG}{dt} \delta V = \frac{\partial (P \delta V)}{\partial t} - P \frac{d(\delta V)}{dt} + \rho \frac{\partial G}{\partial t} \delta V \qquad (17)$$

In fact, it was obtained Eq. (18), from which it was possible to propose a general differential equation under the time domain with the capability to get information on the pressure in the road of the fluid in order to achieve the correlation of the flow with the pressure difference over two points in the fluid road. Furthermore, the correlation between the flow with the pressure difference can give information on the static curve and coefficients that information on the designed sensor parameters [8, 10, 11]:

$$\delta V \frac{d}{dt} \left(\rho \frac{1}{2} v^2 + P + \rho G \right) = \frac{\partial (P \delta V)}{\partial t} - P \frac{d(\delta V)}{dt} + \rho \frac{\partial G}{\partial t} \delta V \qquad (18)$$

The second member of Eq. (18) is zero, while it is analyzed by conservative force, and it is possible to get Eq. (19), which is quite important for designing the algorithm of the smart sensor because it gives the difference between pressure and the fuel flow by Bernoulli in the theoretical model [8, 10, 11]:

$$\rho \frac{1}{2} v^2 + P + \rho G = constant \qquad (19)$$

3. Modeling

It was necessary to prepare a mathematical model to obtain the optimal estimations of the fuel flow. For this reason, it was worked using the measured values and keeping as reference value the fuel flow achieved by theoretical analysis that can be calculated either by Bernoulli or a calibrated sensor.

The Eq. (20) gives information of the estimated fuel flow "Q_{est}", this result depends on the measured flows that are stored by the "X" matrix, and furthermore, this equation depends on the estimation coefficient "β".

$$Q_{est} = X\beta \tag{20}$$

On the other hand, the expression of "β" is replaced in Eq. (21); hence, it was possible to correlate the estimated fuel flow with a reference value of fuel flow [8, 10, 11]:

$$Q_{est} = X(X^T X)^{-1} X^T Q_{ref} \tag{21}$$

Although fuel flow taken as a reference is given by Eq. (22), another theoretical model instead of the model chosen based on Bernoulli can be achieved, which is given by a model solved from Eq. (18). Even though, for Eqs. (18) and (22), there are parameters dependent on the geometry and material of the designed smart sensor, such as the constant "K" in Eq. (22), proportionate information of the geometrical and material characteristics of the passive components of the designed smart sensor:

$$Q_{ref} = \left[\sqrt{\frac{\Delta P}{K}} \right] \tag{22}$$

In fact, the **Figure 3** depicts the designed algorithm for the smart sensor, in which "Q_{mxn}" is the matrix information of the measured fuel flow in dimension "*mxn*," "ΔP_{mxn}" is the difference of pressure matrix in dimension "*mx1*", the matrix of the internal smart sensor is given by "X_{mxn}", which needs the theoretical fuel flow "Qt_{mxn}", as a consequence, the algorithm give optimal estimated fuel flow to the user by the matrix "Qe_{mxn}".

4. Sensor design

The present chapter is a consequence of the previous considerations analysis, for which the characteristics of the designed smart sensor are analyzed in order to be used in some gas measurement alarms, as well as in applications that seek enhancement of hydrogen combustion motors.

There were prepared samples based in AAO because of the simplicity of getting organized nanoholes by anodization, previously an electrochemical cleaning that was given by electropolishing. The porosity is a good property according to warrant the nanoholes obtained by the anodization [12, 13]; in this context, Eqs. (23)–(26) can give the mathematical explanation to achieve an approximation for the porosity measurement. Hence, Eq. (23) is the volume for a cylindrical solid with side base "l" and height "L":
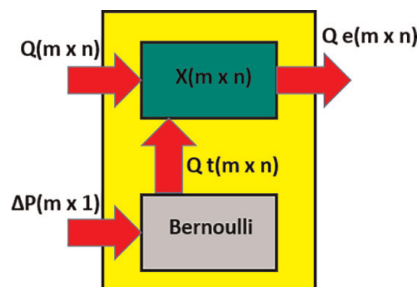

Figure 3.
Block diagram for the algorithm of the designed smart sensor.

$$V_b = \frac{6\sqrt{3}}{4} l^2 L \tag{23}$$

Furthermore, the porous volume is given by Eq. (24), for which the porous diameter is "D_p", and height "L":

$$V_p = \frac{\pi}{4} D_p^2 L \tag{24}$$

Hence, the porosity is achieved from Eqs. (23) and (24), which is shoed by Eq. (25):

$$P = \frac{\frac{\pi}{4} D_p^2 L}{\frac{6\sqrt{3}}{4} l^2 L} \tag{25}$$

In fact, the diameter of the porous "Dp" and the base diameter "Db" proportionate the porosity calculation. In which, it was replaced "l" as a function of "Db" which is described by the Eq. (26):

$$P = \frac{2\pi D_p^2}{3\sqrt{3} D_b^2} \tag{26}$$

Figure 4 depicts a nanohole prepared in a sample of aluminum, the relation of the diameters "Dp" and "Db" are also represented in this figure, moreover the expected hexagon of the AAO holes, which are references to get optimal designs during the anodization.

The chemical equations can explain the hexagon geometry of the nanoholes obtained after the anodization. Hence, Eq. (27) gives the information about the aluminum composition after taking three electrons from its last orbital:

$$Al = Al^{3+} + 3e \tag{27}$$

The chemical equation for water composition is given by Eq. (28):
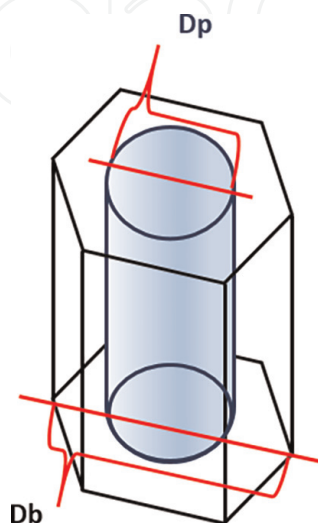
Figure 4.
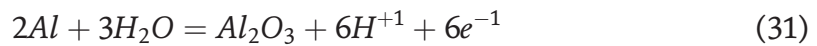*Representation of a nanohole prepared in samples of aluminum.*

$$H_2O = O^{-2} + 2H^{+1} \tag{28}$$

Moreover, it is obtained Eq. (29) by the reaction between aluminum and oxygen:

$$2Al^{+3} + 3O^{-2} = Al_2O_3 \tag{29}$$

From Eqs. (28) and (29), it is achieved Eq. (30):

$$2Al^{+3} + 3H_2O = Al_2O_3 + 6H^{+1} \tag{30}$$

Replacing Eq. (27) in (30) helped to get Eq. (31), which gives the information of the AAO obtaining:

$$2Al + 3H_2O = Al_2O_3 + 6H^{+1} + 6e^{-1} \tag{31}$$

After designing nanoholes over aluminum samples, there were prepared structures (amorphous nanostructures) based on electrochemical deposition by materials such as titanium, silver, gold, and silicon. **Figure 5** shows a picture that was taken from a microscope Litz on a scale of 25 μm. In which are shown some amorphous nanoparticles with an average diameter of 1000 nm.

The **Figure 6** depicts the designed smart sensor representation. "NS" is the component of the sensor that is covered by nanostructures around the sections "TR" and the samples based in nanotubes to receive the static pressures "P1" and "P2", these samples are integrated as part of the transducer to get the static pressure and they are represented by "NT". Therefore, the transduced signal is used by the microcontroller of the designed smart sensor "SS" aiming to be organized by matrices of static difference of pressure "ΔP", as well as to obtain the optimal estimations of the measured fuel flow and detector alarm that it is measured hydrogen flow and presence of other molecules, such as for example oxygen or mixing of hydrocarbons. In fact, the measured signal can be transmitted by wireless signals "EW1" to external users in order to get diagnostic of the ICM, and the interpretation of the ICM operation that can be achieved by the integration of the solid components of the designed smart sensor.

The nanotubes of the designed transducers are based on Anodic Aluminum Oxide, achieved by electropolishing and anodizing aluminum in high purity. Over the AAO
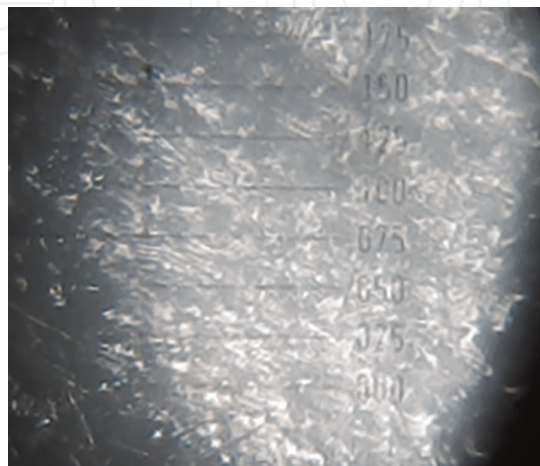

Figure 5.
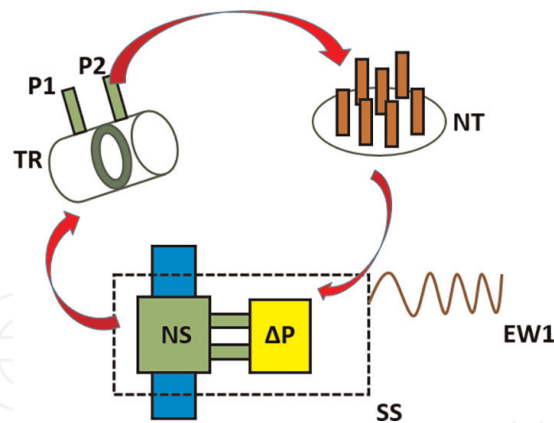*Amorphous nanostructures prepared over AAO, a photo taken by microscope Litz.*

Figure 6.
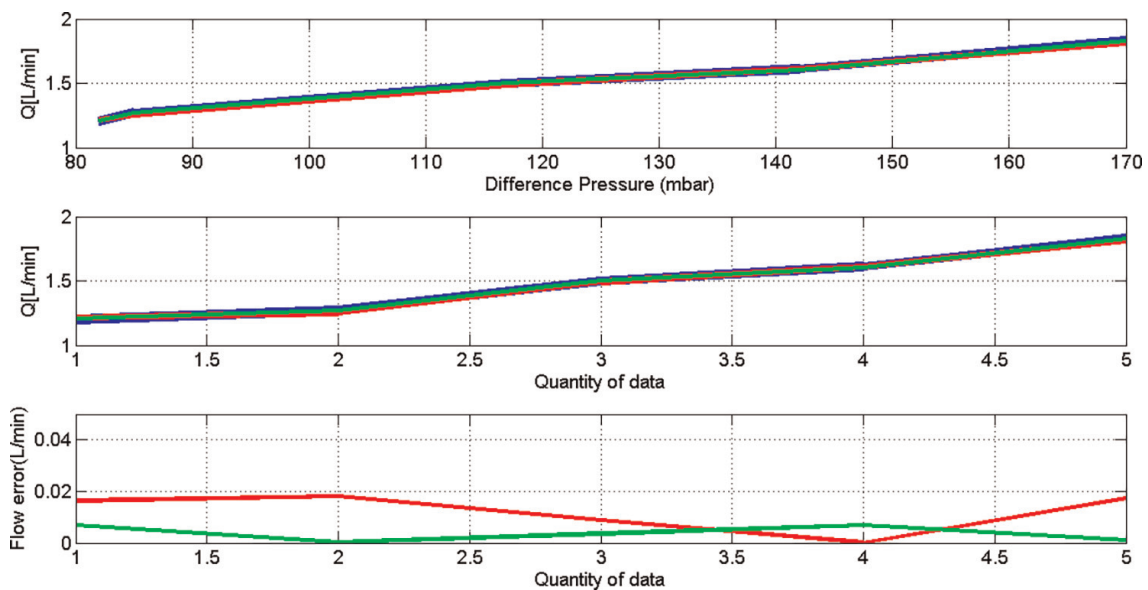*Designed smart sensor representation.*

Figure 7.
Static curve analysis.

samples were focused nano holes according to prepare nanotubes by chemical load deposition, getting transducer samples based in titanium, carbon, silver, gold, and silicon. In order to represent the relation between the fuel flow with the difference of pressure, as it was analyzed in the chapter above, the static curve is given on the **Figure 7** (as well as there are also shown the curves of the flow in dependence on the data quantity), where the blue color curve is based on the measurement supported by the automobile own sensors in which was made the tests (Nissan Frontier 2003). The red color curve is obtained by the theoretical analysis described in this chapter earlier that is supported by Bernoulli analysis; furthermore, the green color curve is the optimal estimation achieved from the designed smart sensor. Hence, in the error comparison of the **Figure 7**, the green color curve is obtained from the comparison between the fuel flow (by the blue color curve in the static analysis of **Q versus ΔP**) with the theoretical fuel flow (by the red color curve in the static analysis of **Q versus ΔP**). Therefore, the green color curve of the error analysis shows that the designed sensor gives optimal fuel flow measurement that also can be used for prediction tasks.
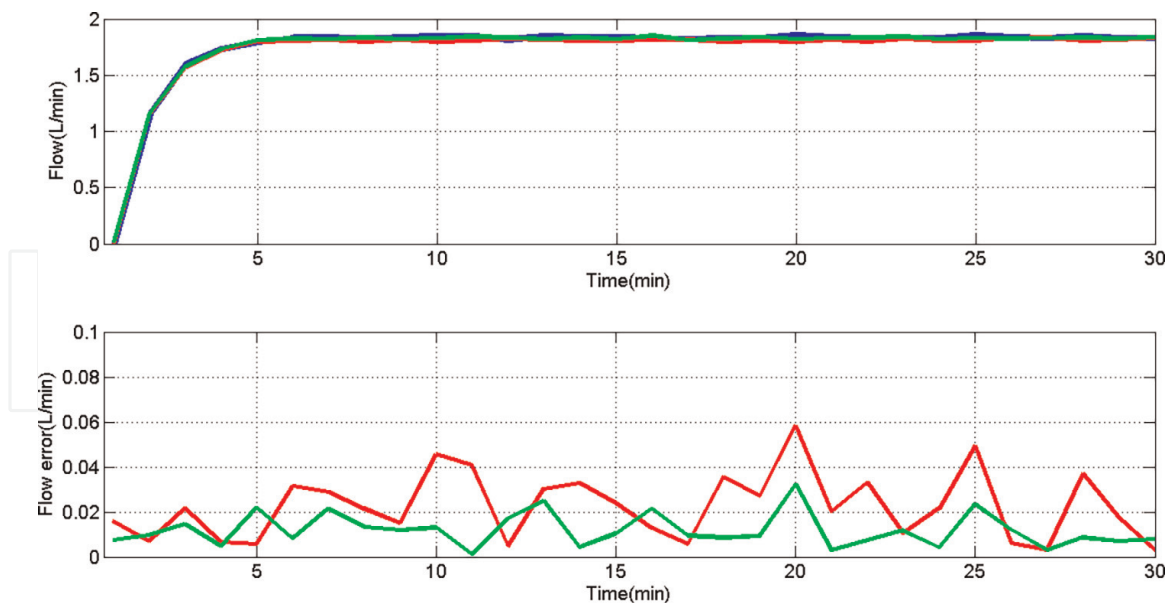
9

Figure 8.
Dynamic curve analysis.

Finally, it was possible to choose an appropriate model for the dynamic analysis of the designed smart sensor response, which was consequently the previous static curve of **Figure** 7, it implies to choose either a linear system analysis by transfer functions or a nonlinear analysis by adaptive modulating functions. The described proposition on the paragraph above is an advantage due to the smart sensor receiving the measured signal in short response time and high robustness for the boundary conditions of the ICM operating point. Therefore, **Figure 8** shows the response of the fuel flow measurement in the time domain (the experiments were done over adaptation in an ICM), in which the blue color curve is obtained by the calibrated sensor (that belongs to the Nissan Frontier), the red color curve is the result of the theoretical analysis, and the green color curve is the optimal flow measurement achieved by the designed smart sensor. Furthermore, there are shown the flow error curves for the dynamical analysis evaluation, in which the red color curve was taken as a consequence of the comparison between the data obtained from the calibrated sensor with the theoretical flow, and the green color curve is the result of the comparison between the data achieved from the calibrated sensor with the data achieved by the designed sensor that got an approximation of 50% less than the error obtained by the theoretical model.

In other hand, there were obtained many alarms of presence of oxygen molecules and hydrocarbon residues in the nonfiltered fuel flow, because of evaluating the performance of the alarm sensor.

5. Conclusions

It was designed a smart sensor with the capability to proportionate to the user's optimal estimations of fuel flow under an ICM operation.

The designed smart sensor measures hydrogen flow as the fuel of the ICM is tested, getting alarms when there is the presence of oxygen and hydrocarbon molecules inside the fuel flow.

The proposed smart sensor is based on transducers of nanostructures working in the operating point of the tested ICM. Furthermore, it helped to achieve a short

response time and high robustness as part of the designed sensor inside the boundary conditions of the ICM operating point.

The polynomial analysis as part of the behavior on the theoretical and experimental models of the fuel flow measurement is a good advantage for the designed smart sensor because it helped to design optimal algorithms to operate nonlinear systems.

6. Future work

It is proposed, as future work, to use the proposed design for tasks in telemetric control in some parameters of the ICM operation.

It is suggested to enhance the algorithm of the designed sensor by an adaptive analysis supported in least mean square on the polynomials of the achieved mathematical models, owing to improve uses of the response time as an advantage achieved from the transducers sensors designed, which are based in nanostructures.

Acknowledgments

A. Appendix

This chapter summarized some of the mathematical demonstrations, which are quite important for the explanation and understanding of the physics laws as part of the designed smart sensor effects [8, 10, 11].

A.1 Looking for the demonstration of Eq. (8)

$$\frac{d}{dt}P = \frac{\partial}{\partial t}P + \frac{d}{dx}P\frac{\partial}{\partial t}\delta x + \frac{d}{dy}P\frac{\partial}{\partial t}\delta y + \frac{d}{dz}P\frac{\partial}{\partial t}\delta z \tag{A1}$$

$$\frac{d}{dt}P = \frac{\partial}{\partial t}P + \frac{d}{dx}Pv_x + \frac{d}{dy}Pv_y + \frac{d}{dz}Pv_z \tag{A2}$$

$$\frac{d}{dt}P = \frac{\partial}{\partial t}P + \frac{d}{dx}Pv_x + \frac{d}{dy}Pv_y + \frac{d}{dz}Pv_z \tag{A3}$$

$$\frac{d}{dt}P = \frac{\partial}{\partial t}P + \nabla P.v \tag{A4}$$

Since

$$\frac{d}{dt} = \frac{\partial}{\partial t} + v.\nabla \tag{A5}$$

B. Looking for the demonstration of the Eq. (9)

$$\frac{d}{dt}\delta V = \frac{d}{dt}[\delta x(\delta y \delta z)] \tag{B1}$$

$$\frac{d}{dt}\delta V = \delta x \frac{d}{dt}(\delta y \delta z) + \delta x \frac{d}{dt}(\delta y \delta z) \tag{B2}$$

$$\frac{d}{dt}\delta V = \delta x \frac{d}{dt}(\delta y \delta z) + (\delta y \delta z)\frac{d}{dt}\delta x \tag{B3}$$

$$\frac{d}{dt}\delta V = \delta x \left[\delta y \frac{d}{dt}(\delta z) + \delta z \frac{d}{dt}(\delta y)\right] + (\delta y \delta z)\frac{d}{dt}\delta x \tag{B4}$$

$$\frac{d}{dt}\delta V = \delta y \delta z \frac{d}{dt}(\delta x) + \delta x \delta z \frac{d}{dt}(\delta y) + \delta x \delta y \frac{d}{dt}(\delta z) \tag{B5}$$

$$\frac{d}{dt}\delta V = \delta y \delta z \, v_x + \delta x \delta z \, v_y + \delta x \delta y \, v_z \tag{B6}$$

$$\frac{d}{dt}\delta V = \delta y \delta z \frac{d}{dx}v_x \delta x + \delta x \delta z \frac{d}{dy}v_y \delta y + \delta x \delta y \frac{d}{dz}v_z \delta z \tag{B7}$$

$$\frac{d}{dt}\delta V = \delta x \delta y \delta z \frac{d}{dx}v_x + \delta x \delta y \delta z \frac{d}{dy}v_y + \delta x \delta y \delta z \frac{d}{dz}v_z \tag{B8}$$

Hence

$$\frac{d}{dt}\delta V = \delta V \, (\nabla.v) \tag{B9}$$

C. Looking for the demonstration of the Eq. (21)

$$Q_{est} = X(X^T X)^{-1} X^T Q_{ref} \tag{21}$$

It must be analyzed

$$J = e^2 \tag{C1}$$

Moreover,

$$J = (Q_{ref} - Q_{est})^T (Q_{ref} - Q_{est}) \tag{C2}$$

Therefore

$$J = \left(Q_{ref} - X\beta\right)^{T} \left(Q_{ref} - X\beta\right) \tag{C3}$$

Also

$$J = \left(Q_{ref}^{T} - \beta^{T}X^{T}\right) \left(Q_{ref} - X\beta\right) \tag{C4}$$

As well as

$$J = Q_{ref}^{T}Q_{ref} - \beta^{T}X^{T}Q_{ref} - Q_{ref}^{T}X\beta + \beta^{T}X^{T}X\beta \tag{C5}$$

It must be remembered

$$Q_{est\,mx1} = X_{mxn}\beta_{nx1} \tag{C6}$$

For which

$$X_{mxn} = [Q_{mx1}(:,1); Q_{mx1}(:,2); \ldots; Q_{mx1}(:,n)]_{mxn} \tag{C7}$$

Furthermore,

$$\beta_{1xn}^{T}X_{nxm}^{T}Q_{ref\,mx1} = number_{1x1} \tag{C8}$$

Looking for its Transpose

$$Q_{ref\,1xm}^{T}X_{mxn}\beta_{nx1} = number_{1x1} \tag{C9}$$

Therefore, comparing Eqs. (C8) and (C9).

$$\beta_{1xn}^{T}X_{nxm}^{T}Q_{ref\,mx1} = Q_{ref\,1xm}^{T}X_{mxn}\beta_{nx1} \tag{C10}$$

It means that in Eq. (C5)

$$J = Q_{ref}^{T}Q_{ref} - 2\beta^{T}X^{T}Q_{ref} + \beta^{T}X^{T}X\beta \tag{C11}$$

It will be used the following properties (C12), (C13), and (C14)

$$\frac{\partial\left(A^{T}X\right)}{\partial X} = A \tag{C12}$$

$$\frac{\partial\left(A^{T}X\right)}{\partial X^{T}} = A^{T} \tag{C13}$$

$$\frac{\partial\left(X^{T}AX\right)}{\partial X} = 2AX \tag{C14}$$

Looking for the minimal value in the Eq. (C11)

$$\frac{\partial J}{\partial \beta} = 0 - 2\frac{\partial}{\partial \beta}\left(\beta^{T}\left(X^{T}Q_{ref}\right)\right) + \frac{\partial}{\partial \beta}\left(\beta^{T}(X^{T}X)\beta\right) \tag{C15}$$

By properties (C13) and (C14) in the Eq. (C15)

$$\frac{\partial J}{\partial \beta} = 0 - 2\frac{\partial\left(\left(X^T Q_{ref}\right)^T \beta\right)^T}{\left(\partial \beta^T\right)^T} + 2(X^T X)\beta \qquad \text{(C16)}$$

In the minimal point

$$0 = -2\left(\frac{\partial\left(\left(X^T Q_{ref}\right)^T \beta\right)}{\partial \beta^T}\right)^T + 2(X^T X)\beta \qquad \text{(C17)}$$

Therefore

$$\left(\left(X^T Q_{ref}\right)^T\right)^T = (X^T X)\beta \qquad \text{(C18)}$$

It means

$$\beta = \left(X^T X\right)^{-1} X^T Q_{ref} \qquad \text{(C19)}$$

Finally, it is achieved

$$Q_{est} = X\left(X^T X\right)^{-1} X^T Q_{ref} \qquad \text{(C20)}$$

Author details

J. Alan Calderón Ch[1,2,3]*, Fernando O. Jiménez U.[2], E. Benjamín Barriga G.[2],
Julio C. Tafur S.[2], Dante J. Gallo T.[2,4], Juan Carlos R. Lengua A.[2], John H. lozano J.[2,4,5]
and Hugo Lozano Núñez[6]

1 Applied Nanophysics, Institute for Physics, Technical University of Ilmenau,
Ilmenau, Germany

2 Control Engineering and Automation Master Program, Mechatronic Engineering
Master Program, Energy Laboratory, Engineering Department, Pontifical Catholic
University of Peru, Peru

3 Aplicaciones Avanzadas en Sistema Mecatrónicos JACH S. A. C, Peru

4 Control System Department, Continental University, Huancayo, Junín, Peru

5 Northen (Artic) Federal University named after MV Lomonosov, Russian
Federation

6 Electrical System Department, Central University of Huancayo, Huancayo, Junín,
Peru

*Address all correspondence to: alan.calderon@pucp.edu.pe

IntechOpen

References

[1] Optris. Infrared Thermometers: Basic Principles of Non-Contact Temperature Measurement. GmbH Germany

[2] T. E. Sensor Solutions. TS318-11C55 Thermopile Sensor 2015.

[3] Texas Instruments. Designing a Low-Cost. High-Accuracy Infrared Thermometer; 2020

[4] NDT, Tek Know. Innovative Technologies. Non Destructive Devices Control. 2015. Available from: www.tek-know.ru; https://tek-know.ru/upload/ib lock/709/7096fe2e53a35d1455399881fd 4c8785.pdf

[5] He J-H, Liu D-P, Chung C-H, Huang H-H. Infrared thermography measurement for vibration-based structural health monitoring in low-visibility harsh environments. Sensors MDPI. 2020

[6] Zhang F, Jiang M, Zhang L, Ji S, Sui Q, Chenhui S, et al. Internal combustion engine fault identification based on FBG vibration Sensor and support vector machines algorithm. Hindawi Mathematical Problems in Engineering. 2019. DOI: 10.1155/2019/8469868

[7] Christiana B, Volkb J, Lukàcsb IE, Sautieffc E, Sturmd C, Graillote A, et al. Piezo-force and vibration analysis of ZnO nanowire arrays for sensor application. Procedia Engineering. 2016

[8] Person AE. Aerodynamic Parameter Estimation via Fourier Modulating Function Techniques, Brown University, NASA Contractor Report 4654. 1995

[9] Alan Calderón J, Barriga B, Tafur J, Lozano J, Lengua JC, Solano G, et al. Optimal vibration analysis for a combustion motor. In: IEEE Conference on Industrial Electronics and Applications (ICIEA). 2021

[10] Landau LD, Lifshitz EM. Theory of Elasticity, Course of Theoretical Physics. Vol. 7. Institute of Physical Problems, USSR Academy of Science; 1959

[11] Richard F, Robert L, Matthew S. The Feynman Lectures on Physics. Vol. I. New Millennium Editors; 1962

[12] Lei Y, Cai W, Wilde G. Highly ordered nanostructures with tunable size, shape and properties: A new way to surface nano-pattern in using ultrathin alumina masks. Progress in Materials Science. 2007;**52**(4):465-539. DOI: 10.1016/j.pmatsci.2006.07.002

[13] Sieber M. Elektrochemisches Modell zur Beschreibung der Konversion von Aluminium durch anodische Oxidation. 2016